

Analysis of PA 6 nanocomposites – indentation and creep behavior as a function of temperature and load level using different indentation techniques

Jan Schöne^{1), *)}, David Tondl²⁾, Ralf Lach^{3), 4)}, Jan Rybnicek^{2), 5)}, Wolfgang Grellmann^{1), 3), 4)}

DOI: dx.doi.org/10.14314/polimery.2014.722

Abstract: The short-term performance (Martens hardness and indentation modulus) and the time-dependent creep behavior of polyamide 6 (PA 6) and two PA 6 nanocomposites containing 3.5 wt % montmorillonite (MMT) or 5 wt % halloysite nanotubes (HNT) were analyzed by different depth-sensing indentation techniques in the nano-, micro- and macro-range of loading as a function of applied load (0.08–100 N) and temperature (-80–60 °C). Additionally, WAXD and DSC measurements were made to establish the morphology-property relationships of the investigated materials while taking into account the skin-core structure of the injection-moulded samples.

Keywords: depth-sensing indentation techniques, Martens hardness, indentation modulus, creep behavior, skin-core effect, temperature, polyamide 6, nanocomposites.

Analiza zależności twardości i pełzania pod obciążeniem nanokompozytów PA 6 od temperatury i siły obciążającej oraz od głębokości zagłębiania

Streszczenie: Za pomocą techniki DSI (*Depth Sensing Indentation*), z zastosowaniem głębokości wciskania z zakresu nano, mikro oraz makro, analizowano zależność twardości indentacyjnej, twardości Martensa, modułu wciskania oraz pełzania pod obciążeniem nanokompozytów poliamidu 6 od temperatury (-80–60 °C) i przyłożonej siły (0,08–100 N). Badano nanokompozyty PA 6 napełnione montmorylonitem (3,5 % mas.) oraz nanorurkami haloizytu (5 % mas.). Dodatkowo przy użyciu technik WAXD oraz DSC oceniano wpływ morfologii badanych materiałów na ich właściwości, z uwzględnieniem efektu *skin-core* w próbkach otrzymanych metodą wtryskiwania.

Słowa kluczowe: metoda DSI pomiaru twardości, twardość Martensa, moduł wciskania, pełzanie pod obciążeniem, efekt *skin-core*, poliamid 6, nanokompozyty.

In the last two decades, polymer nanocomposites based on inorganic minerals have attracted a great deal of attention. Polyamide 6 (PA 6) materials have become particularly increasingly important for the automotive industry and other sectors producing construction parts.

Polyamide nanocomposites offer good chemical, scratch, heat and wear resistance combined with a good surface appearance. Furthermore, nanocomposites exhibit significant enhancements of properties such as enhanced mechanical properties, reduced gas permeability, increased thermal stability and improved flame retardancy [1–13]. The influence of nanofillers on the crystal modification has been analyzed by many research groups [6–12, 14–19].

Recently, analyses have been carried out on how the properties of various polyamides such as PA 6 are affected by halloysite nanotubes and nanoclays. Marney *et al.* [2] studied the influence of different halloysite fractions as a fire retardant on PA 6 materials. They found that halloysite nanotube filler contents of 15 wt % results in optimal fire retardant properties, but with the optimal content for the mechanical properties is much lower than 15 wt % HNT. Liu *et al.* [17], who investigated PA 6/montmorillonite, found that a filler content of close to 3 wt % was optimal. Similarly, Seltzer *et al.* [20] found 3.3 wt % organoclay in a PA 6 matrix to be an optimum loading.

¹⁾ Polymer Service GmbH Merseburg, Geusaer Straße Geb. 131, 06217 Merseburg, Germany.

²⁾ Czech Technical University in Prague, Faculty of Mechanical Engineering, Innovation Centre for Diagnostics and Application of Materials, Technicka 4, 166 07 Prague 6, Czech Republic, e-mail: david.tondl@seznam.cz

³⁾ Martin-Luther University Halle-Wittenberg, Centre of Engineering, 06099 Halle/Saale, Germany, e-mail: wolfgang.grellmann@iw.uni-halle.de

⁴⁾ Institute of Polymer Materials, Geusaer Straße Geb. 131, 06217 Merseburg, Germany, e-mail: ralf.lach@psm.uni-halle.de

⁵⁾ Centre of Excellence Prague s.r.o., Kocova 513/22, 181 00 Prague 8, Czech Republic, e-mail: jrybnicek@gmail.com

^{*)} Author for correspondence; e-mail: jan.schoene@iw.uni-halle.de

These two studies state independently that the mechanical properties partly decrease with increasing filler loading above the optimal value.

Another key aspect is an influence on the mechanical and thermal properties PA 6 of crystal modification. Montmorillonite and halloysite nanotubes prefer the formation of the metastable γ -phase inside PA 6. Furthermore, the halloysite nanotubes act as nucleation agents [5].

A benefit of the present work is to highlight the sensitivity of different hardness measurement systems applied to the analysis of the morphology-dependent mechanical properties. Injection-moulded PA 6 samples possess a skin-core structure [21, 22] and, consequently, the mechanical responses in the skin and core regions are different [19, 23]. However, most studies of different polyamide materials are limited to the nano- or micro-range of loading, investigating the hardness only for low indentation depths at room temperature [15, 17–20, 24–29]. A major disadvantage in these studies is that the skin-core effect cannot be analyzed without time-consuming cutting and polishing of the samples to expose new surfaces. In contrast, the use of macrohardness measuring systems makes it possible to disregard the erroneous shape of the indenter tip, the stress concentration inside the tested sample just behind the indenter tip (causes the so-called indentation size effect) and small-sized surface effects (such as the skin-core structure and the surface roughness) due to higher indentation depths resulting from the higher load level. So far, to the best knowledge of the authors of the present study, there have been no investigations of the mechanical performance of polyamide materials as a function of temperature using macroindentation techniques. First, we adapted a temperature chamber and a temperature controller for the macrohardness tester Zwick ZHU 2.5. This provided the instrument to determine the macrohardness and other mechanical properties dependent on the temperature [30]. In the present study, the Martens hardness, indentation modulus and creep behavior were analyzed as a function of nanofiller (halloysite nanotubes and montmorillonite), the morphology of the PA 6 matrix (crystal modification and crystallinity), as a function of load (ranging from 0.08 N to 100 N using different hardness testers) and temperature (-80 °C, 23 °C and 60 °C).

EXPERIMENTAL PART

Materials

The neat PA 6, a commercial product with the trade name SCAAMID PA 6 B140, was produced by Polykemi AB (Sweden). The commercially available PA 6/montmorillonite (MMT) nanocomposite, produced as SCAN-COMP PA 6 B140 A6 by Polykemi AB (Sweden), contains 3.5 wt % nanosized MMT platelets. The PA 6/HNT nanocomposite is a compound of Pleximer N (NaturalNano,

USA) and neat PA 6 [Pleximer-N being the masterbatch of PA 6 Balamid B3K (BASF) with 30 wt % halloysite nanotubes (HNT)]. The filler fraction of PA 6/HNT investigated in this study was 5 wt %.

Preparation of samples

To study the mechanical behavior, dumbbell-shaped specimens according to ISO 527 (specimen type 1A) were injection molded using a Battenfeld 500 machine. Before testing, all samples were conditioned according to ISO 1110, which results in moisture content equal to that of long-term conditioning in air at 23 °C and 50 % relative humidity.

Methods of testing

Differential scanning calorimetry (DSC)

The DSC curves were recorded for temperatures ranging from 0 °C to 300 °C by means of a DSC 820 device (Mettler-Toledo, Switzerland). Generally, both the heating and cooling rate were set to 10 deg/min. The weight of the samples was 1–6 mg. The α -phase peak temperature of the second heating run was defined as the melting temperature T_m and, similarly, that of the cooling run as the crystallization temperature T_{pc} . In both cases, the peak areas were used to calculate the melting or crystallization enthalpy (ΔH_m or ΔH_c), respectively. By considering the melting enthalpy ΔH_m^0 of 100 % crystalline PA 6 ($\Delta H_m^0 = 241 \text{ J/g}$ of α -phase PA 6 and $\Delta H_m^0 = 239 \text{ J/g}$ of γ -phase PA 6, respectively [31]), the degree of crystallinity X_c of neat PA 6, PA 6/MMT and PA 6/HNT was estimated by $X_c = \Delta H / \Delta H_m^0 \cdot 100\%$, where ΔH_m designated as ΔH was approximated to 100 per cent matrix material.

Wide-angle X-ray diffraction (WAXD)

WAXD analyses were performed for neat PA 6 and the nanocomposites using an URD 63 diffractometer (Seifert-FPM, Germany), Ni-filtered CuK_α radiation ($\lambda = 0.15418 \text{ nm}$) and a scintillation counter for registration. The measurements were conducted in a transmission geometry and stepped scan mode at room temperature (23 °C).

Hardness measurement techniques

In the nano-range of loading, all materials were analyzed by a Nanotest (Micromaterials Ltd., UK) at room temperature (23 °C). The maximum load was fixed at 80 mN and the application time was 20 s; the duration time of the load-controlled creep test was fixed at 60 s.

In the micro-range of loading, the measurements were done using a Fischerscope H100c (Helmut Fischer GmbH, Germany) at room temperature (23 °C), where the maximum load was set to 1 N. The other measuring

parameters were the same as in the nano-range of loading.

Finally, in the macro-range of loading, a Zwick ZHU 2.5 macrohardness testing machine (Zwick/Roell GmbH & Co. KG, Germany) was equipped with a temperature chamber and temperature controller [30]. The measuring parameters were the same as applied in the nano- and micro-range again except for the maximum loads, which were 10 N and 100 N. However, the creep behavior and hardness properties were measured at lower and higher temperatures (-80 °C and 60 °C) than room temperature (23 °C).

The relative humidity of the air in the laboratory was generally 50 %.

Independent of the range of loading used (nano, micro or macro), load (F) vs. indentation depth (h) diagrams were obtained both in the loading and unloading regime from which the Martens hardness HM and the indentation modulus E_{IT} were calculated according to ISO 14577-1:2002 (for more information see [32, 33], for example). The indentation creep C_{IT} (in %) is defined as the ratio of the increment in indentation depth after the duration time and the indentation depth after the application of the load. For each data point, 5–10 $F-h$ or indentation depth vs. time diagrams were analyzed.

RESULTS AND DISCUSSION

Crystallization behavior

In Figure 1 the cooling and second heating runs of the neat PA 6 and the nanocomposites are shown, respectively. Table 1 summarizes the crystallization and melting temperatures (T_{pc} and T_m), as well as the degree of crystallinity X_c based on analyzing the DSC curves. The temperature T_g of the broad glass transition (not shown in Fig. 1b) is found to be about 48–51 °C, almost unaffected by the incorporation of nanoparticles into PA 6.

The half width of the crystallization peak of neat PA 6 is less than that of PA 6/HNT (Fig. 1a) while T_{pc} of both materials is nearly the same ($T_{pc} = 190$ –191 °C, see Table 1). However, the dispersed halloysite nanotubes inside PA 6/HNT promote the crystallization slightly due to a possible nucleation effect (according to the shift of the crystallization peak in Fig. 1a). Since PA 6/MMT has a broader crystallization peak than the other materials, it exhibits a lower crystallization temperature ($T_{pc} = 186$ °C).

Figure 1b, the second heating runs of the materials, shows the double-peak shape of the melting region typical for PA 6 materials, where the first peak (at lower temperatures) is correlated with the γ -phase of PA 6 and the second peak (at higher temperatures) with the α -phase, respectively. On closer inspection, the presence of MMT results in shifting the α -phase melting peak to a slightly lower temperature (219 °C) compared to that of neat PA 6 and PA 6/HNT (220 °C). Whereas the nucleation effect of HNT on the PA 6 matrix (see above) has also been determined by Prashantha *et al.* [4] and Guo *et al.* [5], the deg-

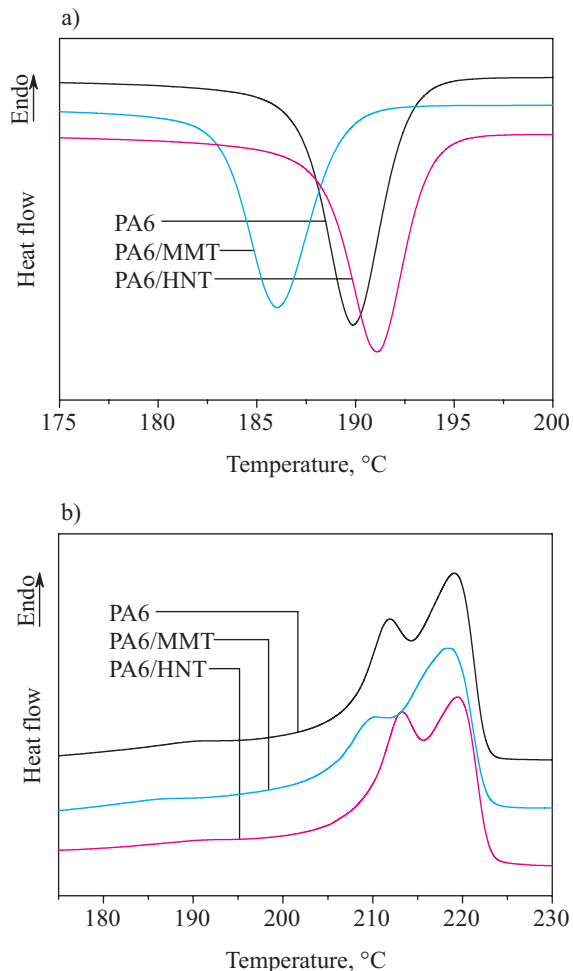


Fig. 1. DSC curves: a) cooling and b) second heating runs of PA 6 and nanocomposites PA 6/MMT, PA 6/HNT

ree of crystallinity is a somewhat controversial issue. At the same heating rate of 10 deg/min as used in this study, Prashantha *et al.* [4] and Guo *et al.* [5] stated that the addition of HNT to the PA 6 matrix led to an increase or a decrease in the degree of crystallinity. In the present study, however, the degree of crystallinity remained nearly unaffected by the incorporation of HNT (and MMT) into PA 6 (Table 1), *i.e.* the degree of crystallinity of PA 6 was only insignificantly higher than that of the nanocomposites. The unaffected degree of crystallinity using nanoclay, *i.e.* MMT in our case, agrees with DSC measurements reported in the literature [23].

Table 1. DSC properties of neat PA 6 and its nanocomposites

Samples	T_{pc} , °C	T_m , °C	ΔH , J/g	X_c , %
PA 6	190	220	74.6	31.1
PA 6/MMT	186	219	72.7	30.3
PA 6/HNT	191	220	73.0	30.4

Figure 2 describes the results of the WAXD measurements. In neat PA 6, the stable α -crystal modification is

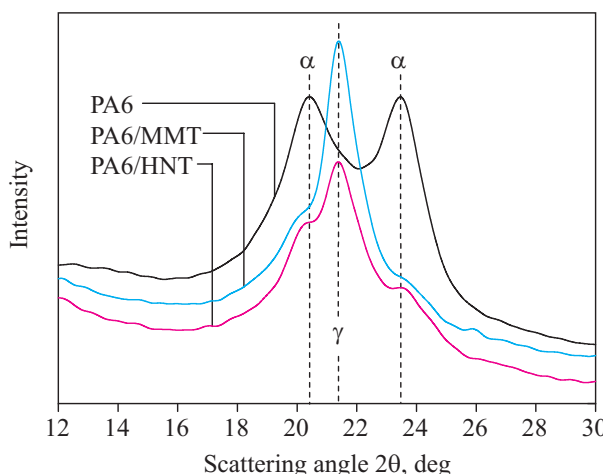


Fig. 2. WAXD results of PA 6 and nanocomposites PA 6/MMT, PA 6/HNT

dominant, but the metastable γ -modification still exists (compare Fig. 1b). The matrix in both PA 6 nanocomposites consists mostly of the γ -modification (in PA 6/MMT more than in PA 6/HNT) and only to a less degree of the α -phase. These findings are in accordance with the literature [7, 8, 34].

Indentation results

Figure 3a,b show the values of indentation modulus E_{IT} and Martens hardness HM , respectively, of the PA 6

materials depending on the applied load level. For both neat PA 6 and PA 6/HNT, E_{IT} is found to jump to the highest values at a load of 100 N after decreasing first for loads ranging from 80 mN to 10 N. For E_{IT} of PA 6/MMT, there is no clear trend for loads of 0.08–10 N, but the jump in E_{IT} at a load of 100 N is fully comparable to that observed for PA 6 and PA 6/HNT. Neat PA 6 is the softest material without exception and PA 6/MMT is generally the hardest material, notwithstanding its lower filler weight fraction (3.5 wt %) compared with that of PA 6/HNT (5 wt %). Considering that the relative changes in the values are smaller in HM than in E_{IT} , the Martens hardness follows the same trends as the indentation modulus. The pronounced increases in hardness and indentation modulus by dispersion of only small amounts of nanofillers into PA 6 have also been found in the literature [19, 23].

Similar to the discussion in the literature given by Shen *et al.* [19] using a nanoindentation approach, we interpret the jumps in hardness and modulus as a skin-core effect due to the processing (injection moulding). From the depth-dependent measurements in [19], indentation modulus and hardness, we found an increase from the surface (skin) to the core inside the samples of neat PA 6 and PA 6 containing 5 and 10 wt % nanoclay. Before measuring, the samples were cut and polished to expose new surfaces. The temperature gradient from the skin to the core inside the freshly injection-moulded samples results in the formation of γ - and α -phases in the skin and core, respectively (see WAXD measurements of the skin and

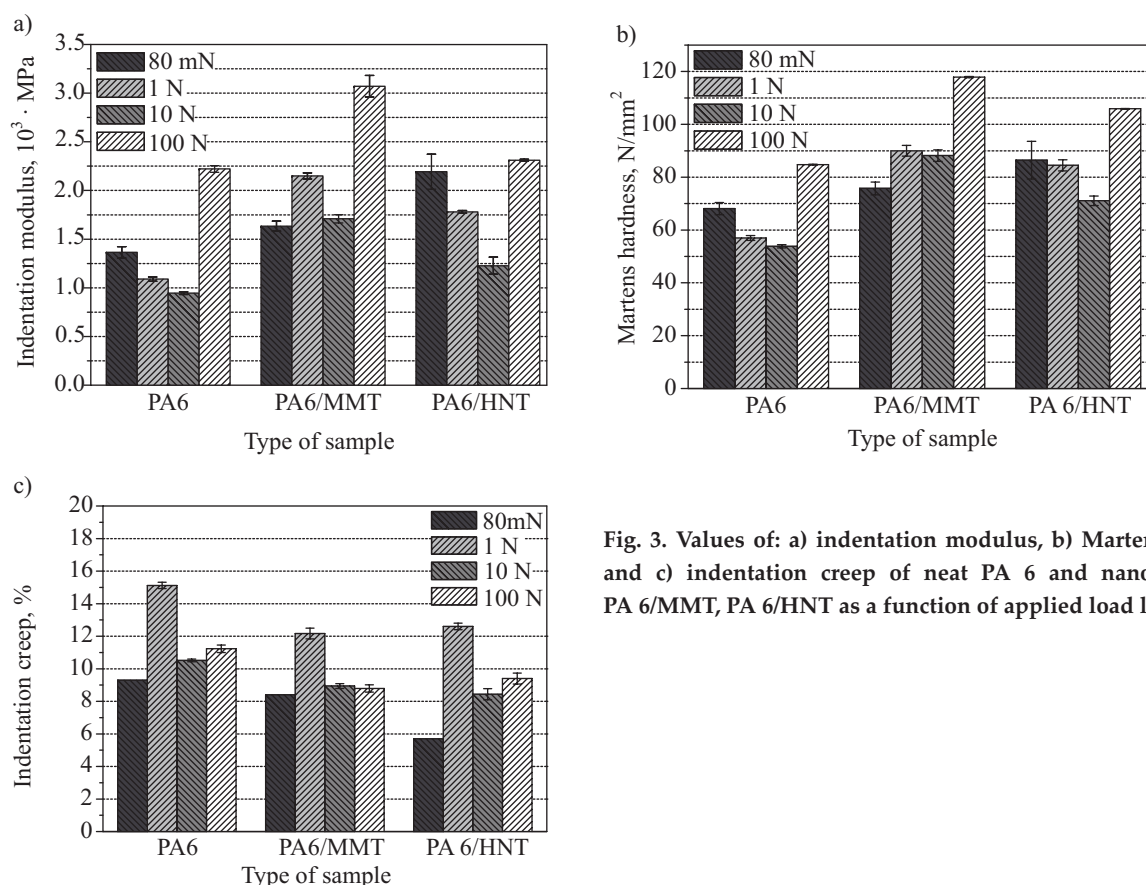


Fig. 3. Values of: a) indentation modulus, b) Martens hardness and c) indentation creep of neat PA 6 and nanocomposites PA 6/MMT, PA 6/HNT as a function of applied load level

core region in [23]). As is well known, the modulus of the α -phase is higher than that of the γ -phase [15, 36, 36] underlining the skin-core effect observed in [19] and the present study. Nanoindentation tests by Seltzer *et al.* [19, 20, 23] on neat PA 6 and PA 6/nanocomposites (2.5–10 wt % organoclay) also indicated a distinct skin-core effect in the nanocomposites (no effect was observed for neat PA 6); however, higher values of indentation modulus were found in the skin than in the core. Therefore, the occurrence of the skin-core effect may be dependent on the ratio of α - to γ -crystallites, both in the skin and core, counteracted by molecular orientation in the neat polyamide and by molecular, nanofiller and crystal orientation in the nanocomposites [23].

Figure 3c shows the results of the load level-dependent indentation creep tests at room temperature. Interestingly, the highest indentation creep values of each material are correlated with a load of 1 N and the lowest values with a load of 80 mN. This behavior may provide an indication of depth-dependent changes in morphology (as shown in [20]) sensitive to the creep behavior as a function of the load level. Studying neat PA 6 and nanoclay containing PA 6 materials, Seltzer *et al.* [19, 20, 23] also found depth-dependent creep properties. Like [19,

finishing and the influences of cutting and polishing across surfaces, the application of recording macroindentation testing to analyse the short-term and time-dependent mechanical performance of polymer material forms the basis of identifying depth-sensing properties (such as the skin-core effect) in detail. The L_2 VH method [32, 33] is an alternative method to conventional nanoindentation measurements to analyse the hardness perpendicular to the mould direction across the specimen thickness. The so-called Vickers hardness under load (*i.e.* L_2 VH) was calculated by applying the following steps: (i) transformation of the loading branch of the $F-h$ diagrams measured into $F/h-h$ curves, (ii) differentiation of these $F/h-h$ curves: $a(h) = \partial(F/h)/\partial h$, (iii) calculation of L_2 VH: L_2 VH(h) = $a(h)/26.43$ (L_2 VH in N/mm^2 , load F in N, indentation depth h in mm). Fig. 4a shows the results of the cross section macroindentation measurements across the sample thickness, where the maximum load was fixed to be 400 N. It is clearly shown that the L_2 VH method is a good alternative to identify the depth-sensing properties without any cutting and sample finishing. Furthermore, the L_2 VH method is independent of the applied load. The conventional nanohardness method across the sample thickness (Fig. 4b) and the more straightforward L_2 VH

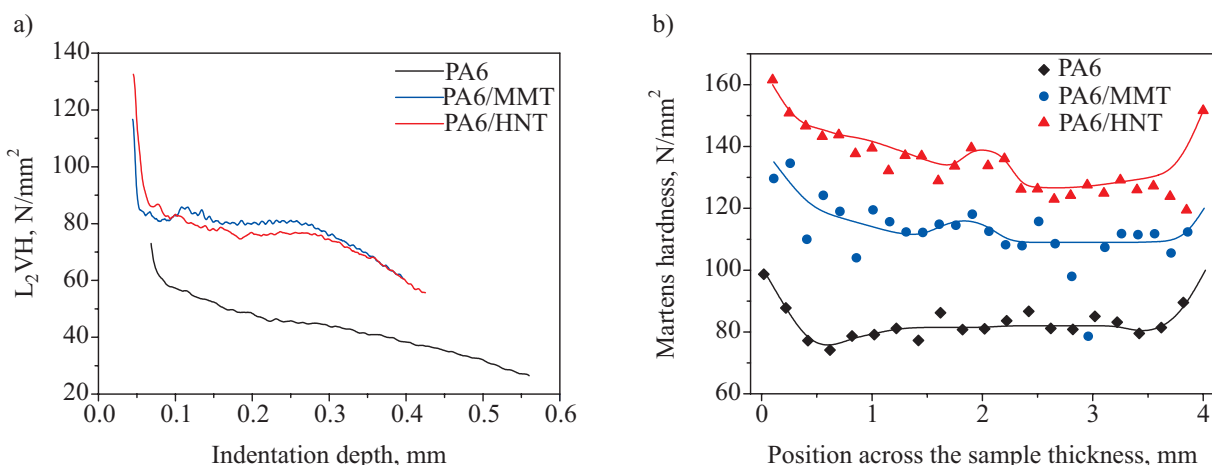


Fig. 4. L_2 VH vs. indentation depth profiles – a) and nanohardness depending on the cross section position across the specimen thickness – b) of neat PA 6 and nanocomposites PA 6/MMT, PA 6/HNT; the lines in Fig. 4b are fits applying Fast Fourier Transformation (FFT) of the data

23], the injection-moulded samples were cut and polished to expose different surfaces. The observed skin-core effect comprised higher values of creep compliance in the core than in the skin [20]. Furthermore, by incorporation of nanofillers into PA 6, the creep values decreased because both MMT and HNT constrain the mobility of the macromolecules (compare [20]). As a result, the addition of nanofiller (organoclay up to 3.3 vol % [20]) improves the creep resistance of the PA 6 nanocomposites, as found in [20] as well as in the present study.

Due to disadvantages of the nanoindentation techniques mostly used in the literature, including high sample

method lead qualitatively to nearly the same hardness *vs.* depth profile. The larger values of the conventional nanoindentation measurements probably resulted from grinding and polishing of the sample surface. With the L_2 VH method, it is possible to analyse depth-sensing effects (thickness of injection-moulding skin) without time-consuming surface preparation.

Figure 5 summarises the macroindentation results as a function of temperature. The maximum load of all measurements is fixed at 10 N. As expected, both indentation modulus (Fig. 5a) and Martens hardness (Fig. 5b) decrease with increasing temperature. The indentation

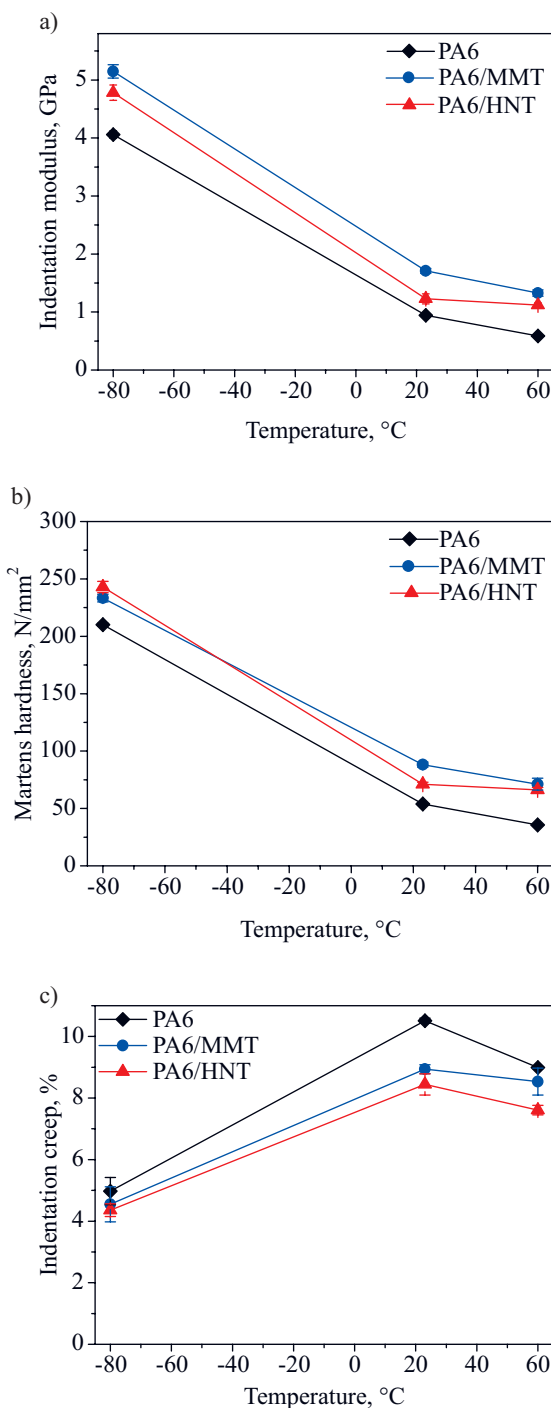


Fig. 5. Values of a) indentation modulus, b) Martens hardness and c) indentation creep of neat PA 6 and nanocomposites PA 6/MMT, PA 6/HNT as a function of temperature

creep (Fig. 5c) increases up to room temperature (23 °C) and then decreases once again. On the one hand, the modulus and hardness of the nanocomposites are higher than those of the neat PA 6, but on the other hand, the indentation creep is lower. Interestingly, the ranking of the nanocomposites depends on the material parameter to be considered: While HNT highly affects C_{IP} whereas MMT has the highest effect on both HM and E_{IP} . Furthermore, the contrasting behavior of HM as a quantity of the “indentation hardness” was found in one of our recent

papers [38] where the scratch hardness of PA 6/HNT is higher than that of PA 6/MMT due to different microdeformation processes during indentation and scratching.

CONCLUSIONS

Incorporation of nanofillers (regardless of MMT and HNT) into PA 6 results in changing the preferred crystal modification from α to γ . However, the crystallisation and melting temperatures, as well as the degree of crystallinity, are mainly unaffected compared to neat PA 6 except for PA 6/MMT, which has a somewhat lower crystallisation temperature. Furthermore, HNT acts slightly as a nucleation agent.

From indentation testing at room temperature, the values of Martens hardness and indentation modulus determined as a function of load (0.08–100 N) have been found to jump at the highest applied load level (*i.e.* 100 N), which has been interpreted as a skin-core effect due to processing, as supported by the literature. The macroindentation measurements as a function of temperature (-80–60 °C) have shown that both the indentation modulus and the Martens hardness decrease with increasing temperature. In comparison, the indentation creep reaches a maximum at room temperature probably due to the glass transition of the amorphous phase inside the polymer matrix or recrystallization. Whereas the nanocomposites exhibit the highest values of modulus and hardness, the nanofillers constrain the indentation creep independent of temperature and load level.

In the present work, it has been demonstrated that data from different indentation techniques has to be examined carefully to be comparable. In addition, depth-dependent information about the local mechanical behavior can be easily obtained by using different indentation techniques without any time-consuming surface preparations of the samples.

ACKNOWLEDGMENTS

The authors wish to thank the German Research Foundation (DFG) for financial support. Furthermore, they thank Prof. Dr. Androsch (Martin-Luther University Halle-Wittenberg) and Dr. Wutzler (Polymer Service GmbH Merseburg) for the DSC and WAXD tests.

REFERENCES

- [1] Wang S., Hu Y., Li Z., Wang Z., Zhuang Y., Chen Z., Fan W.: *Colloid Polym. Sci.* **2003**, 281, 951. <http://dx.doi.org/10.1007/s00396-002-0858-x>
- [2] Marney D.C.O., Russell L.J., Wu D.Y., Nguyen T., Cramm D., Rigopoulos N., Wright N., Greaves M.: *Polym. Degrad. Stab.* **2008**, 93, 1971. <http://dx.doi.org/10.1016/j.polymdegradstab.2008.06.018>
- [3] Sikdar D., Katti D., Katti K., Mohanty B.: *J. Appl. Polym. Sci.* **2007**, 105, 790. <http://dx.doi.org/10.1002/app.26284>

- [4] Prashantha K., Schmitt H., Lacrampe M.F., Krawczak P.: *Compos. Sci. Technol.* **2011**, *71*, 1859.
<http://dx.doi.org/10.1016/j.compscitech.2011.08.019>
- [5] Guo B., Zou Q., Lei Y., Du M., Liu M., Jia D.: *Thermochim. Acta* **2009**, *484*, 48.
<http://dx.doi.org/10.1016/j.tca.2008.12.003>
- [6] Ishisue T., Okamoto M., Tashiro K.: *Polymer* **2010**, *51*, 5585.
<http://dx.doi.org/10.1016/j.polymer.2010.09.033>
- [7] Katoh Y., Okamoto M.: *Polymer* **2009**, *50*, 4718.
<http://dx.doi.org/10.1016/j.polymer.2009.07.019>
- [8] Maiti P., Okamoto M.: *Macromol. Mater. Eng.* **2003**, *288*, 440.
<http://dx.doi.org/10.1002/mame.200390040>
- [9] Dencheva N., Denchev Z., Oliveira M.J., Funari S.: *J. Appl. Polym. Sci.* **2007**, *103*, 2242.
<http://dx.doi.org/10.1002/app.25250>
- [10] Feng M., Gong F.L., Zhao C., Chen G., Zhang S., Yang M.: *Polym. Int.* **2004**, *53*, 1529. <http://dx.doi.org/10.1002/pi.1593>
- [11] Goitisolo I., Eguiazabal J.I., Nazabal J.: *Polym. Degrad. Stab.* **2008**, *93*, 1747. <http://dx.doi.org/10.1016/j.polymdegradstab.2008.07.030>
- [12] Karaman V.M., Privalko V.P., Privalko E.G., Lehmann B., Friedrich K.: *Macromol. Symp.* **2005**, *221*, 85.
<http://dx.doi.org/10.1002/masy.200550309>
- [13] Gallego R., García-Lopez D., Merino J.C., Pastor J.M.: *Polym. Int.* **2010**, *59*, 472. <http://dx.doi.org/10.1002/pi.2724>
- [14] Androsch R., Stolp M., Radusch H.J.: *Acta Polymerica* **1996**, *47*, 99. <http://dx.doi.org/10.1002/actp.1996.010470206>
- [15] Shen L., Phang I.Y., Liu T.: *Polym. Test.* **2006**, *25*, 249.
<http://dx.doi.org/10.1016/j.polymertesting.2005.09.019>
- [16] Aldousiri B., Dhakal H.N., Onuh S., Zhang Z., Bennett N.: *Polym. Test.* **2011**, *30*, 688. <http://dx.doi.org/10.1016/j.polymertesting.2011.05.008>
- [17] Liu S.-P., Hwang S.-S., Yeh J.-M., Hung C.-C.: *Int. Commun. Heat Mass Transfer* **2011**, *38*, 37.
<http://dx.doi.org/10.1016/j.icheatmasstransfer.2010.10.003>
- [18] Shen L., Phang I.Y., Liu T., Zeng K.: *Polymer* **2004**, *45*, 8221.
<http://dx.doi.org/10.1016/j.polymer.2004.09.062>
- [19] Shen L., Tjiu W.C., Liu T.: *Polymer* **2005**, *46*, 11 969.
<http://dx.doi.org/10.1016/j.polymer.2005.10.006>
- [20] Seltzer R., Mai Y.-W., Frontini P.M.: *Compos., Part B: Eng.* **2012**, *43*, 83. <http://dx.doi.org/10.1016/j.compositesb.2011.04.035>
- [21] Fornes T.D., Paul D.R.: *Polymer* **2003**, *44*, 3945. [http://dx.doi.org/10.1016/S0032-3861\(03\)00344-6](http://dx.doi.org/10.1016/S0032-3861(03)00344-6)
- [22] Yu Z.-Z., Yang M., Zhang Q., Zhao C., Mai Y.-W.: *J. Polym. Sci., Part B* **2003**, *41*, 1234.
<http://dx.doi.org/10.1002/polb.10480>
- [23] Seltzer R., Frontini P.M., Mai Y.-W.: *Compos. Sci. Technol.* **2009**, *69*, 1093. <http://dx.doi.org/10.1016/j.compscitech.2009.01.029>
- [24] Shen L., Phang I.Y., Chen L., Liu T., Zeng K.: *Polymer* **2004**, *45*, 3341. <http://dx.doi.org/10.1016/j.polymer.2004.03.036>
- [25] Shen L., Wang L., Liu T., He C.: *Macromol. Mater. Eng.* **2006**, *291*, 1358. <http://dx.doi.org/10.1002/mame.200600184>
- [26] Mishra S., Sonawane S.S., Shimpi N.G.: *Appl. Clay Sci.* **2009**, *46*, 222. <http://dx.doi.org/10.1016/j.clay.2009.07.024>
- [27] Rajeesh K.R., Gnanamoorthy R., Velmurugan R.: *Mater. Sci. Eng. A* **2010**, *527*, 2826.
<http://dx.doi.org/10.1016/j.msea.2010.01.070>
- [28] Regrain C., Laiarinandrasana L., Toillon S.: *Eng. Fract. Mech.* **2009**, *76*, 2656. <http://dx.doi.org/10.1016/j.engfrac-mech.2009.04.016>
- [29] Sinha S.K., Song T., Wan X., Tong Y.: *Wear* **2009**, *266*, 814.
<http://dx.doi.org/10.1016/j.wear.2008.12.010>
- [30] Lach R., Schöne J., Bierögel C., Grellmann W.: *Macromol. Symp.* **2012**, *315*, 125. <http://dx.doi.org/10.1002/masy.201250516>
- [31] Illers K.-H.: *Makromol. Chem.* **1978**, *179*, 497.
<http://dx.doi.org/10.1002/macp.1978.021790224>
- [32] Fröhlich F., Grau P., Grellmann W.: *Physica status solidi (a)* **1977**, *42*, 79. <http://dx.doi.org/10.1002/pssa.2210420106>
- [33] May M., Fröhlich F., Grau P., Grellmann W.: *Plaste Kautschuk* **1983**, *30*, 149.
- [34] Fornes T.D., Paul D.R.: *Macromolecules* **2004**, *37*, 7698.
<http://dx.doi.org/10.1021/ma0487570>
- [35] Miyasaka K., Isomoto T., Koganeya H., Uehara K., Ishikawa K.: *J. Polym. Sci., Part A-2* **1980**, *18*, 1047.
<http://dx.doi.org/10.1002/pol.1980.180180511>
- [36] Tashiro K., Tadokoro H.: *Macromolecules* **1981**, *14*, 781.
<http://dx.doi.org/10.1021/ma50004a060>
- [37] Rybnicek J., Lach R., Dominguez S.R., Tondl D., Valek R., Grellmann W.: *RFP — Rubber Fibres Plastics International* **2013**, *8*, 40.

Received 11 VII 2013.

Revised version 28 III 2014.